*Journal of Sound and Vibration* (1998) **215**(5), 1183–1194
*Article No*. sv981639

# STABILITY TO TRANSLATIONAL GALLOPING VIBRATION OF CYLINDERS AT DIFFERENT MEAN ANGLES OF ATTACK

S. C. Luo, Y. T. Chew, T. S. Lee and M. G. Yazdani†
*Department of Mechanical and Production Engineering*, *National University of Singapore*, 10 *Kent Ridge Crescent*, *Singapore* 119260

(*Received* 23 *October* 1997, *and in final form* 2 *March* 1998)

## 1. INTRODUCTION

Flow-induced vibration of structures in a flow is an important problem in fluid mechanics; it is also both a challenging fundamental problem and one that has important application potential. To date, a number of mechanisms responsible for flow-induced vibration have been identified; one of them is the transverse translational galloping vibration of structures. Traditionally (see references [1, 2]), the square cylinder has been (and still is) the most popular shape employed in galloping oscillation research. The majority of them, which include work reported in references [3–5], is focused on the special case when the mean angle of attack ($\alpha$) is zero. In reality, one should not be confined to just one cross-sectional shape, and there is no reason why galloping stability at non-zero degree mean angle of attack should not receive as much attention as the zero degree (special) case. By examining the sign of the slope of the normal force coefficient ($C_N$) versus $\alpha$ plot obtained in a steady flow experiment, with positive $\partial C_N/\partial\alpha$ indicating instability to transverse translational galloping and vice versa, Luo *et al*. [6] suggested that prismatic bodies with other cross-sectional shapes may also be unstable to transverse galloping, and shapes that are stable to transverse galloping at one particular mean $\alpha$ may not remain to be so at another mean $\alpha$. The main objective of the work reported in the present paper is, by building upon the work reported in reference [6], to further investigate the effects of cross-sectional geometry and mean angle of attack on the stability to cross-flow translational galloping vibration of a prismatic cylinder via dynamic (cylinder force-oscillated transversely to the free stream) experiments.

## 2. EXPERIMENTAL ARRANGEMENT

### 2.1. *Experimental set-up*

All the tests were conducted in an open loop wind tunnel with a test section of 1 m ($W$) $\times$ 0·6 m ($H$) $\times$ 2·75 m ($L$). In the present work most of the data were acquired within the free stream speed ($U$) range of 3–10 m/s. At a free stream speed of 10 m/s, the streamwise turbulence intensity of the flow is less than 0·5%.

In order to investigate the effects of cross-sectional geometry systematically, cylinders with four different cross-sectional geometries were employed in the present investigation. The cross-sectional geometry includes a square, two symmetrical trapeziums and an isosceles triangle. All of them share identical streamwise and cross-stream dimensions ($d$) of 50 mm. The rear sides of the two symmetrical trapeziums have dimensions of $3d/4$ and $d/2$, and will from now on be referred to as trapeziums 1 and 2, respectively. For the triangular cylinder, the vertex of the isosceles triangle always points in the downstream

† Present address: School of Engineering, Temasek Polytechnic, 21 Tampines Avenue 1, Singapore 529757.

0022–460X/98/351183 + 12 $30.00/0 

direction. Figure 1 shows a summary of all the four cross-sectional geometries, and the positive directions of various quantities like axial and normal forces and rotation of the cylinder. For the direct measurement of the axial and normal forces (and hence the drag and lift forces), seven evenly spaced pressure taps were installed at mid-span on all the four sides of the square cylinder. For the other three cylinders, two different sets of pressure taps (one for direct normal force and the other for direct axial force measurement) were installed 5 mm away (one on each side) of the mid-span position. For direct normal force measurement, seven evenly spaced pressure taps were installed on both the side faces of the cylinder. On the other hand, for direct axial force measurement, seven and six spaced pressure taps were installed on the front face of the two trapezoidal cylinders and the triangular cylinder, respectively. The pressure taps on the other three faces were located by the projection of the front face pressure taps in the axial force direction. The pressure averager technique was adopted for the direct measurement of the mean pressure on each face of the cylinder. Depending on the number of pressure taps on each face, either six to one or seven to one pressure averagers were used. The pressure signals (output of the pressure averagers) were measured by pressure transducers positioned just outside the test section via fairly long PVC pressure transmitting tubings. The pressure transducers used are Setra 239 ($\pm 0{\cdot}1$ p.s.i. $= \pm 689{\cdot}5$ Pa) differential pressure transducers. The outputs of the pressure transducers were in turn fed to an Intel 486 based PC that was equipped with Metrabyte DAS20 data acquisition and SSH-4 sample and hold cards for multi-channel simultaneous on-line data acquisition. Normal and axial forces were derived by differencing the mean pressure on the two side faces and the mean pressure on the front and rear faces, respectively. More information about the pressure averager technique can be found in references [5, 7].

In order to suppress undesirable spanwise flow, $10d$ (streamwise) $\times$ $8d$ rectangular end plates were installed on both ends of the cylinder. The end plates were installed such that the distance between the leading edges of the end plates and the front side of the cylinder is $2{\cdot}5d$. The spanwise distance between the two end plates was $9{\cdot}2d$.

In the present investigation, the cylinder that was installed vertically inside the test section was force-oscillated in a direction transverse to the free stream by a twin

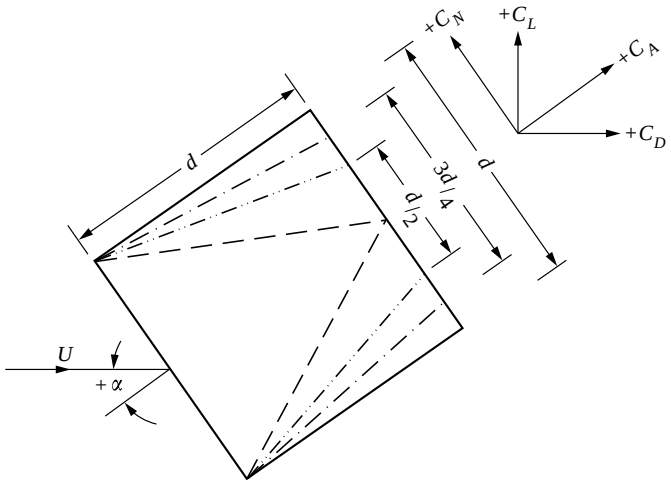


Figure 1. Dimensions of cross-sections and directions of positive quantities ($d = 50$ mm): —, square; – – –, trapezium 1; – – – – –, trapezium 2; - - - , triangle.

Scotch–Yoke mechanism, which were in turn driven by a motor through some gearing system. By varying the motor speed, the frequency of oscillation ($f_N$) of the cylinder could be changed, and by varying the connecting point between the motor and the Yoke, the amplitude of oscillation of the cylinder ($a$) could also be changed to various discrete values. The displacement of the cylinder was measured by a Schlumberger DC 150 displacement transducer.

### 2.2. *Experimental methodology*

In the present investigation, $a/d$ was kept constant at 1. On the other hand, $f_N$ and $U$ were varied in the range of 1–5 Hz and 3–10 m/s, respectively. Based on the cylinder's characteristic dimension of $d = 50$ mm, the reduced velocity ($U_r = U/(f_N d)$) varied from 12 to 200 and the Reynolds number ($\mathrm{Re} = (\rho U d)/\mu$, where $\rho$ and $\mu$ are the density and dynamic viscosity of the fluid, respectively) varied from $9{\cdot}4 \times 10^3$ to $3{\cdot}1 \times 10^4$.

During each run of data sampling at a particular combination of $U$, $f_N$ ($U_r$ is thus decided), $\alpha$ and $a/d$, the axial and normal force signals (output of two Setra 239 differential pressure transducers) and the cylinder displacement signal (output of the displacement transducer) were measured simultaneously by the PC via DAS 20 data acquisition and SSH4 simultaneous sample and hold cards. In each sampling run, 4096 samples of each signal were acquired at a rate of 200 Hz. With the axial and normal forces measured simultaneously, the instantaneous lift and drag forces acting on the cylinder can also be calculated. The above enables the determination of the phase angle ($\varphi$) between the body frequency component of the lift force ($C_L(f_N)$) and the displacement of the cylinder.

### 2.3. *Corrections of various effects*

In the present investigation, the maximum blockage occurs when trapezoidal cylinder 2 is inclined to the free stream at 30°, and the blockage ratio is just under 5·75% which can be considered as fairly small. The small blockage effects, together with the fact that no satisfactory blockage correction method is available for unsteady flow problems, led the authors to decide that no blockage correction should be carried out.

As fairly long PVC tubings were used to transmit pressure signals, the high frequency content of the signals are attenuated and phase shift is introduced. In order to compensate for the effects caused by the tubings, the tubing frequency response correction method first reported in reference [8] and subsequently in reference [9] was used. Essentially, this involves first measuring the frequency response and phase shift of the tubing used in the experiment. Then, FFT (Fast Fourier Transformation) is applied to any pneumatic signal measured via the tubing to obtain its Fourier Series representation. Next, each term in the Fourier Series is corrected in reference to the frequency response and phase shift of the tubing, before IFT (Inverse Fourier Transformation) is performed to the corrected Fourier Series to obtain the corrected (for tubing frequency response) signal. In the present work, the frequency response of the tubing is corrected by the method described above from 0 to 100 Hz. A pneumatic signal free from the effects of the tubing frequency response in the range 0–100 Hz is thus obtained, and calculations can then be performed to obtain the phase angle $\varphi$ mentioned above.

## 3. RESULTS AND DISCUSSIONS

### 3.1. *Background*

As mentioned in section 1, the main objective of the present investigation is to examine the effects of cross-sectional shape and mean angle of incidence on the transverse translational galloping stability of prismatic bodies. The four cross-sectional shapes

investigated are a square, two symmetrical trapeziums and an isosceles triangle. Of the four shapes, there are already quite a large quantity of data on the square cylinder in the literature. Measurements carried out on the square cylinder in the present work are therefore mainly for the purpose of calibrating the present experimental set-up, and more attention will be paid to the other three shapes. The variation of the mean normal force coefficients with angle of incidence had been reported in reference [6]. For the ease of reference, this $C_N$ versus $\alpha$ plot is reproduced here as Figure 2(a). Since the sign of $\partial C_N/\partial\alpha$ in the static tests' data determines the stability of the body to transverse translational galloping, information on $\partial C_N/\partial\alpha$ (i.e., the gradient of the $C_N$ versus $\alpha$ curve at different $\alpha$) is extracted from Figure 2(a) and plotted against $\alpha$ as Figure 2(b). In Figure 2(b), it

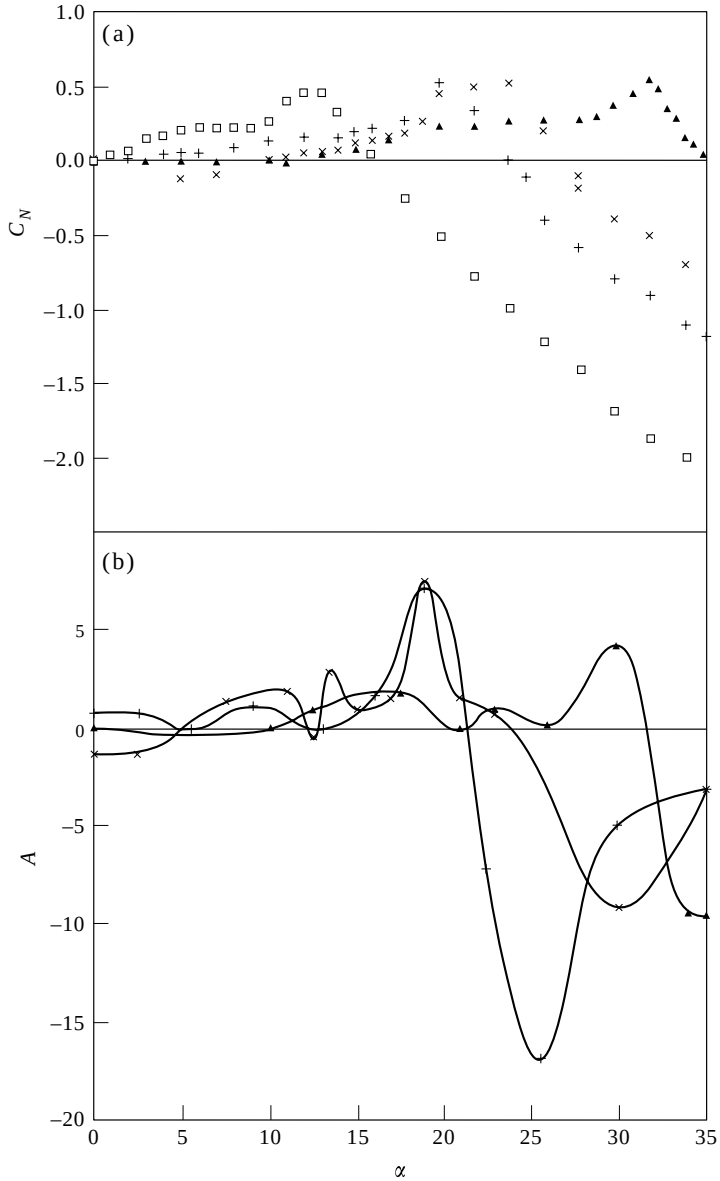


Figure 2. (a) $C_N$ versus $\alpha$; (b) $A$ $(=\partial C_N/\partial\alpha)$ versus $\alpha$. □, square; +, trapezium 1; ×, trapezium 2; ▲, triangle.

should be noted that while the symbols represent actual experimental data points, they were joined by smooth curves and thus the accuracy of points on the curves (which are not actual experimental data) should be interpreted with caution. To examine the effects of angle of incidence, $\varphi$ was measured at $\alpha = 0^\circ$ for the square cylinder (mostly for the purpose of calibrating the experimental set-up and methodology), at $\alpha = 0$, 5, 10, 15 and $18^\circ$ for trapezoidal cylinder 1, at $\alpha = 0$, 5, 10, 14, 20 and $30^\circ$ for trapezoidal cylinder 2, and at $\alpha = 0$, 5, 10, 15, 22, 28 and $32^\circ$ for the triangular cylinder. The above $\alpha$'s were strategically selected so that all the important parts of the $C_N$ versus $\alpha$ curves (positive slope, near zero slope and negative slope etc.) in Figure 2(a) are covered.

For flows that involve sharp edge/corner flow separation, the flow separation positions are fixed, and usually Reynolds number effects (if any) will not be significant. This is especially so in an experiment like the present one as the Reynolds number range is rather small ($9{\cdot}1 \times 10^3$ to $3{\cdot}1 \times 10^4$). All the results discussed below are thus plotted against the reduced velocity ($U_r$) which is generally regarded as the more important parameter in flows that involve a forced oscillated cylinder.

### 3.2. *$\varphi$ versus $U_r$*

As defined earlier, $\varphi$ is the phase angle between the body frequency component of the lift force ($C_L(f_N)$) and the cylinder displacement ($y$). When $\varphi$ is between 0 and $180^\circ$, the body frequency component of the lift force has a component that is in the same direction of the cylinder's velocity, thus leading to instability to transverse galloping. The sign and magnitude of $\varphi$ is thus a useful indicator on the transverse galloping stability of the prismatic body.

$\varphi$ versus $U_r$ data for prismatic cylinders with square, trapezoidal 1, trapezoidal 2 and triangular cross-sections are shown in Figures 3(a)–(d), respectively. For the square cylinder, the present $\varphi$ data (at $\alpha = 0^\circ$) are such that at low $U_r$, $\varphi$ is negative and increases rapidly with $U_r$ until about $70^\circ$, during which $\varphi$ crosses from the negative into the positive region at $U_r \approx 20$. At $\varphi \approx 70^\circ$, the rate of increase of $\varphi$ with $U_r$ reduces, and $\varphi$ asymptotically approaches the quasi-steady value of $90^\circ$ at very high $U_r$. For comparison, the similar data reported in reference [5] which were acquired in a totally independent experiment, are also included in Figure 3(a). The agreement between the two sets of data is found to be good, thus confirming the adequacy of the present experimental set-up and methodology.

For trapezoidal cylinder 1 (Figure 3(b)) at $\alpha = 0^\circ$, $\varphi$ is negative at low $U_r$. $\varphi$ increases with $U_r$ and at $U_r \approx 20$, $\varphi$ becomes positive. $\varphi$ continues to increase with further increase in $U_r$ and reaches a maximum of about $130^\circ$ at $U_r \approx 60$. Beyond that, $\varphi$ decreases with $U_r$ and approaches $90^\circ$ at $U_r > 100$. It can therefore be said that at $\alpha = 0^\circ$, trapezoidal cylinder 1 is unstable to transverse galloping when $U_r$ exceeds 20. At $\alpha = 5^\circ$, $\varphi$ starts from about $-120^\circ$ at $U_r = 12$, gradually increases with $U_r$ and becomes positive when $U_r$ exceeds about 115. It can therefore be said that at $\alpha = 5^\circ$, trapezoidal cylinder 1 is unstable to transverse galloping when $U_r$ exceeds about 115. At $\alpha = 10$ and $15^\circ$, $\varphi$ for both cases remains close to zero (slightly positive most of the time) throughout the $U_r$ range investigated, suggesting that trapezoidal cylinder 1 is weakly unstable to galloping at these $\alpha$'s. At $\alpha = 18^\circ$, $\varphi \approx 130^\circ$ at low $U_r$, decreases with increasing $U_r$, and approaches the quasi-steady value of $90^\circ$ at $U_r \geqslant 50$. It thus appears that at $\alpha = 18^\circ$, trapezoidal cylinder 1 is unstable to transverse galloping within the $U_r$ range ($\approx$10–200) investigated.

For trapezoidal cylinder 2 (Figure 3(c)), it is observed that at mean $\alpha = 0$, 5 and $30^\circ$, $\varphi$ is negative throughout the $U_r$ range investigated, suggesting that trapezoidal cylinder 2 is stable to transverse galloping at those $\alpha$'s. On the other hand, at $\alpha = 20^\circ$, the reverse

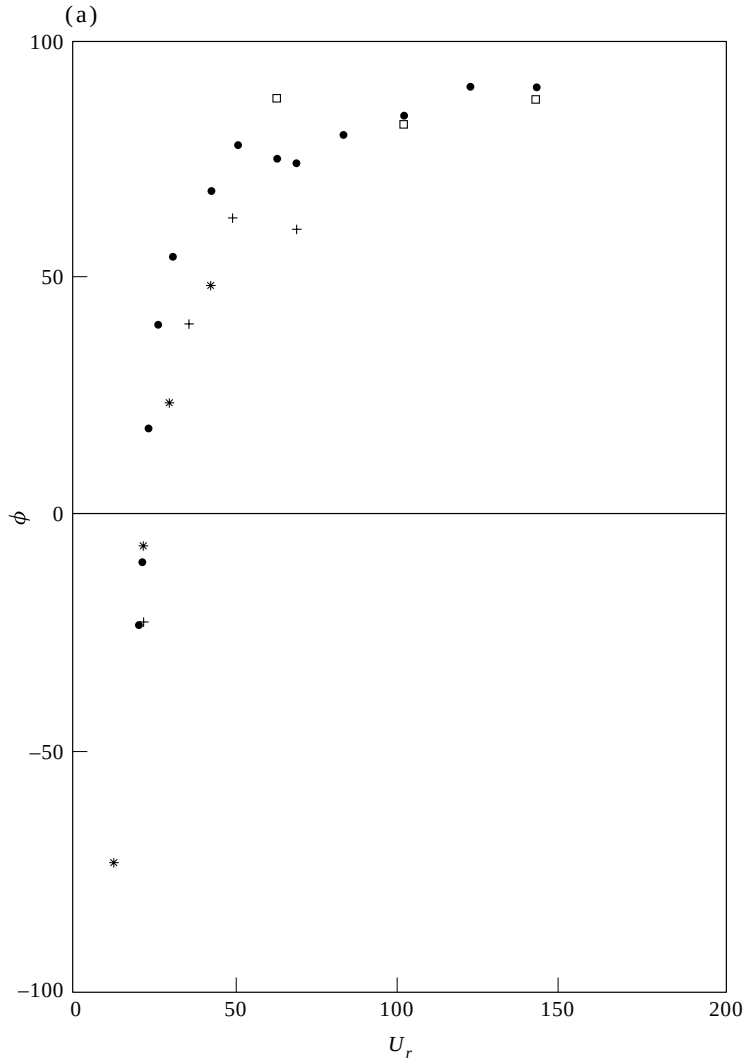


Figure 3(a). *Caption on p*. 1192.

is the case and $\varphi$ is positive (unstable) throughout the $U_r$ range investigated. At $\alpha = 10$ and 14°, trapezoidal cylinder 2 is found to be unstable if $U_r$ exceeds $\approx 30$.

For triangular cylinder (Figure 3(d)), throughout the $U_r$ range investigated, it is observed to be stable ($\varphi$ negative) at $\alpha = 0$, 5 and 10°, but unstable ($\varphi$ positive) at $\alpha = 28$ and 32°. At intermediate $\alpha$ of 15 and 22°, the triangular cylinder is unstable to transverse galloping if $U_r$ exceeds approximately 30 and 55, respectively.

In order to have an overview and to examine the existence of systematic trend (if any) in the data, the data discussed above are summarized in Table 1. In Table 1, the $\varphi$ versus $U_r$ data are divided into three categories, and are referred to as S, U and PU. In the first category, S is for "stable". This refers to the situation when the experimentally measured $\varphi$ is negative throughout the $U_r$ range investigated. The second category is opposite to the first, as U means "unstable", and refers to the situation when the experimentally measured $\varphi$ is positive throughout the $U_r$ range investigated. In the final category, PU refers to

TABLE 1

*Stability of cylinders at different mean angles of attack*

| $\alpha$ (degrees) | Square ($U_{cr}$) [A] $\alpha_{re} = 13{\cdot}5^\circ$ $\alpha_s = 0^\circ$ | Trapezoidal 1 ($U_{cr}$) [A] $\alpha_{re} = 20^\circ$ $\alpha_s = 7^\circ$ | Trapezoidal 2 ($U_{cr}$) [A] $\alpha_{re} = 24^\circ$ $\alpha_s = 14^\circ$ | Triangular ($U_{cr}$) [A] $\alpha_{re} = 32^\circ$ $\alpha_s = 26^\circ$ |
|---|---|---|---|---|
| 0 | PU (20) [3·55–4·17] | PU (20) [1] | S [ − 1·3] | S [0] |
| 5 | | PU (115) [0·2] | S [ ≈ 0] | S [≈0] |
| 10 | | U(WEAKLY) [0] | PU (30) [2] | S [0] |
| 14 | | | PU (30) [2] | |
| 15 | | U(WEAKLY) [0] | | PU (30) [1·8] |
| 18 | | U [7] | | |
| 20 | | | U[2] | |
| 22 | | 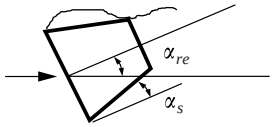 | | P (55) [1·2] |
| 28 | | | | U [2] |
| 30 | | | S [ − 9] | |
| 32 | | | | S [ ≈ 0] |



"partially unstable", and refers to the situation when $\varphi$ is negative at low $U_r$, but becomes positive when a certain $U_r$ is exceeded. The magnitude of $U_r$ at which $\varphi$ first exceeds $0^\circ$ is referred to as the critical reduced velocity ($U_{cr}$) in the present paper. When applicable, the magnitude of $U_{cr}$ is given within curve bracket ( ) in Table 1. The corresponding sign and magnitude of $A(=\partial C_N/\partial\alpha)$ are indicated within square bracket [ ] in Table 1.

By carefully examining Table 1, the following interesting observations are made.

(1) The static experiments predict that the cylinder will gallop if $A$ is positive, while the dynamic experiments suggest galloping instability if $\varphi$ is positive and within the range of 0–180°. The agreement between the two above-mentioned types of prediction is remarkably good, which enhances one's confidence in both types of prediction, in particular the former as it is a prediction of dynamic response based on static tests' results. An even closer examination of the data reveals the following approximate correlations: S:$A \leqslant 0$; PU:$0 < A \leqslant 2$ approximately; and U:$A \geqslant 2$ approximately. These correlations are interesting as they indicate that besides the sign of $A$ obtained from a static test which gives an indication on the stability of a dynamic problem, its magnitude can provide further (approximate) indication on the extent of the instability.

(2) In terms of the magnitude of the mean $\alpha$, it is thought that the flow can be approximately divided into three regimes, as follows.

Low $\alpha$: at low $\alpha$, only cross-sectional shapes that have a substantial afterbody (e.g., square or trapezium 1) are unstable to galloping oscillation. For other shapes, such as trapezium 2 and triangle, because the sides taper away rapidly, the distance between a side and the corresponding separated shear layer is rather large, and that results in insufficient asymmetry in the flow to make galloping instability possible.

Intermediate $\alpha$: as mean $\alpha$ increases, because of the increase in asymmetry, cylinders of all shapes become more unstable. The above means that shapes that are of the PU type at lower $\alpha$ will now become the U type, and shapes that are stable (S type) at lower $\alpha$ will gradually become unstable. A shape that has more afterbody will become unstable at a lower mean $\alpha$ than one that has less afterbody. For example, trapezoidal cylinder 2 is of the S type at mean $\alpha$ of 0 and 5°, it becomes PU at $\alpha = 10^\circ$. On the other hand, the triangular cylinder, which has less afterbody than trapezoidal cylinder 2, behaves as an S type at $\alpha = 0$, 5 and 10°, but becomes the PU type at $\alpha = 15^\circ$. At high intermediate $\alpha$'s which are usually close to the steady flow reattachment angle of the shape concerned ($\alpha_{re}$), shapes may become completely unstable (i.e., U type). This type of flow takes place when reattachment of a separated shear layer onto one side of the cylinder is expected to take

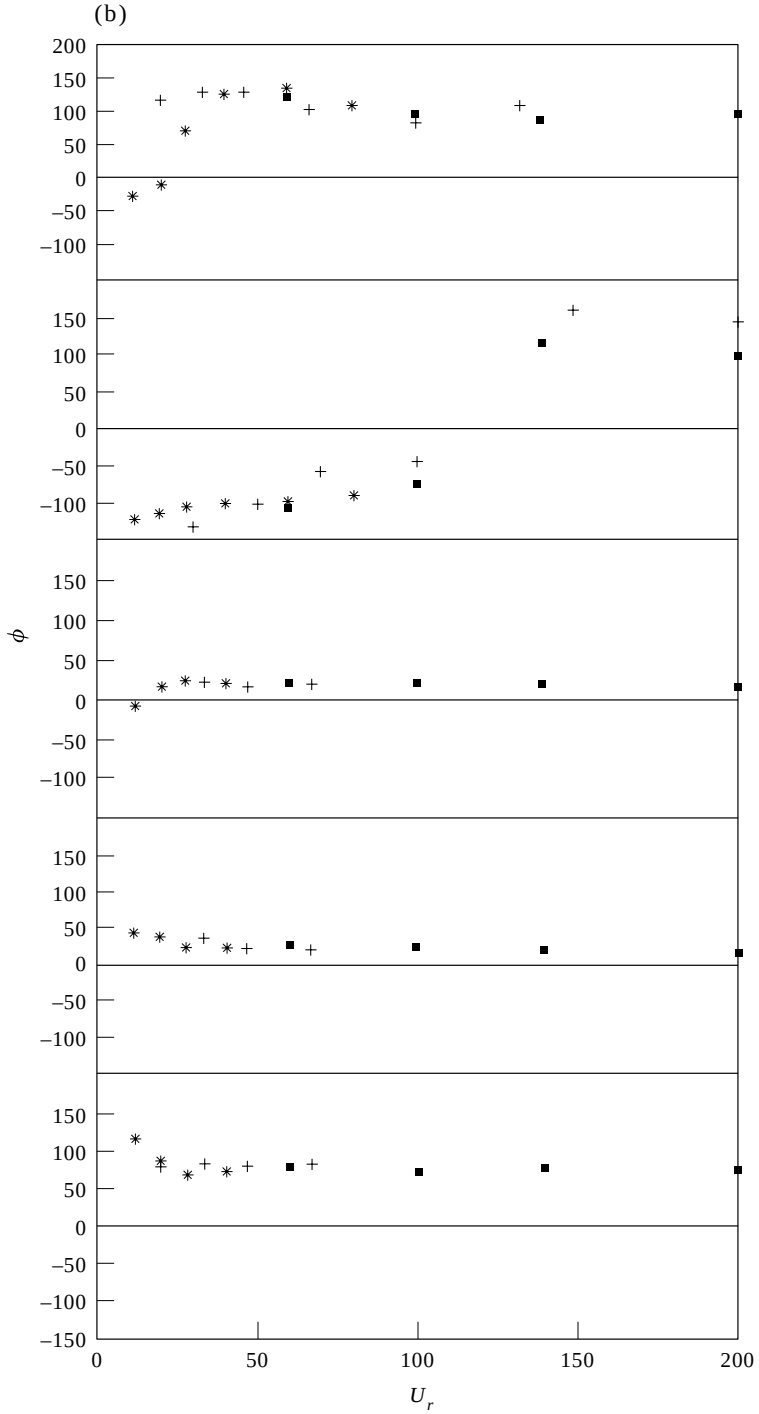


Figure 3(b). *Caption on p*. 1192.

place over a substantial part of the oscillation cycle, and a flow structure that is rather different from those described above is likely to take place. The detailed structure of this type of flow is not clear at present, and how this type of flow leads to a rather unstable situation is an issue that warrants further investigation.

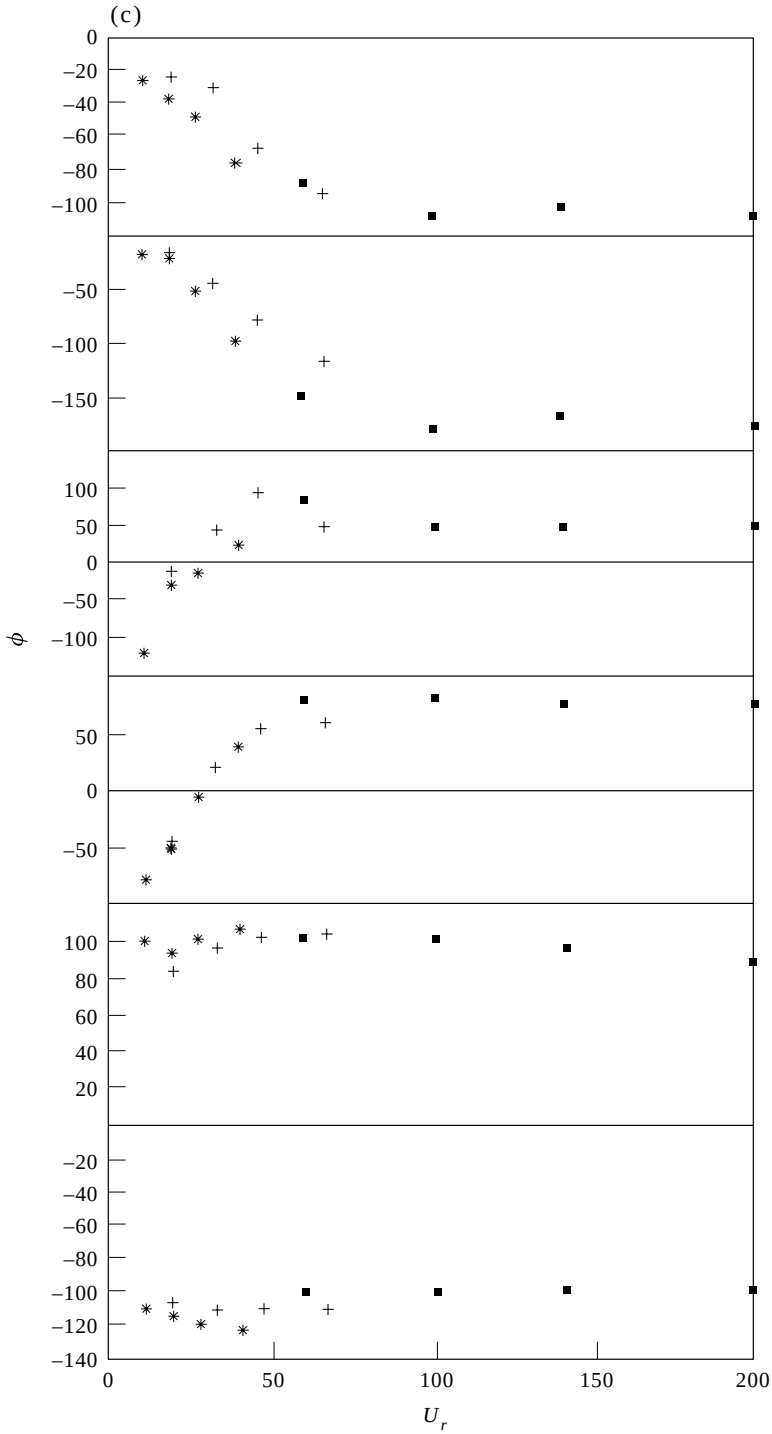


Figure 3(c). *Caption on p*. 1192.

Large $\alpha$: at even larger mean $\alpha$ (typically $\geqslant \alpha_{re}$), the cylinders are gradually becoming stable again (e.g., trapezoidal cylinder 2 at $\alpha = 30^{\circ}$). It is already known but is worth mentioning here that when the mean $\alpha$ is larger than $\alpha_{re}$, one of the separated shear layers

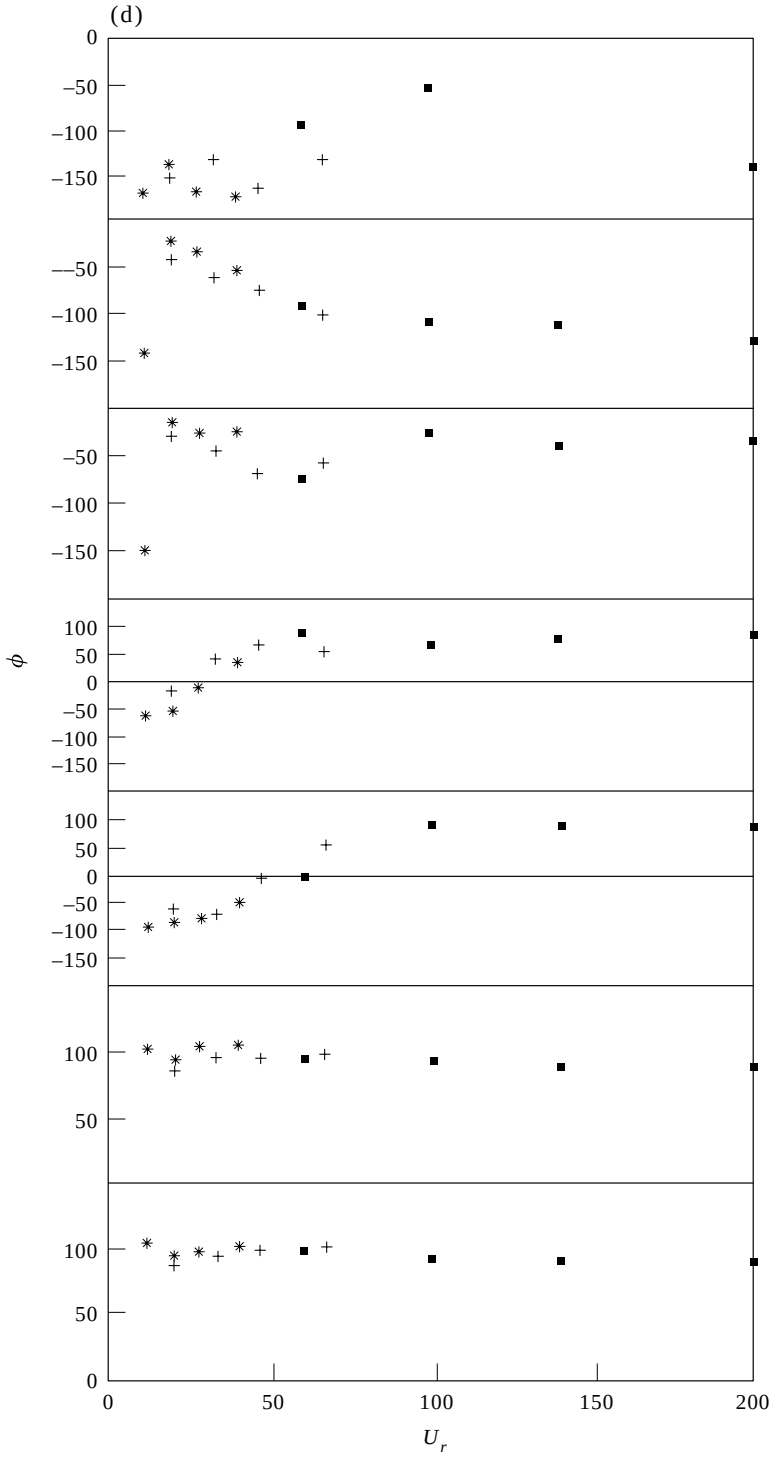


Figure 3(d)

Figure 3. $\varphi$ versus $U_r$, $a/d = 1{\cdot}0$. (a) Square cylinder; $f_N$: □, 1 Hz; +, 3 Hz; ★, 5 Hz; ●, reference [5]. (b) Trapezoidal cylinder 1; $f_N$: ■, 1 Hz; +, 3 Hz; ★, 5 Hz; from top to bottom $\alpha = 0$, 5, 10, 15 and 18°, respectively. (c) Trapezoidal cylinder 2; $f_N$: ■, 1 Hz; –|–, 3 Hz; ★, 5 Hz; from top to bottom $\alpha = 0$, 5, 10, 14, 20 and 30°, respectively. (d) Triangular cylinder; $f_N$: ■, 1 Hz; –|–, 3 Hz; ★, 5 Hz; from top to bottom $\alpha = 0$, 5, 10, 15, 22, 28 and 32°, respectively.

reattaches on the corresponding side of the cylinder, even if it is stationary. It is believed that the reattachment usually leads to stability to transverse galloping. The structure of the flow in this regime also warrants further investigation.

Overall speaking, when $\alpha$ increases from $0^\circ$, the stability (to transverse translational galloping) of the cylinders investigated presently follows the S→PU→U→S transition pattern.

(3) The observation reported in (2) above seems to suggest that the interaction between one side face and its corresponding separated shear layer is sufficient in causing or ending instability to transverse translational galloping.

## 4. CONCLUSIONS

Results of dynamic tests reported in the present paper confirm the findings (from static tests) reported in the authors' earlier paper that probably with the exception of the circular cylinder, the stability to transverse translational galloping of all other prismatic cylinders are both cross-sectional geometry and angle of attack dependent. Due to the increase in suction on a side face caused by an increase in proximity (i.e., getting closer) between that side face and the corresponding separated shear layer when $\alpha$ increases, a prismatic cylinder that is stable at $0^\circ$ or very small mean angle of attack may become unstable at some larger mean angle of attack. The present results, which are obtained from dynamic experiments, also support the adequacy of stability predictions that can be made from static experiments. To a certain extent, the present results also further illustrate the generally known fact that it is the interaction (proximity) between the separated shear layers and the sides of a prismatic body that decides the latter's stability to transverse translational galloping. In fact, the present results show that the interaction between one separated shear layer and the corresponding side is sufficient in deciding the stability of a prismatic body. The present results also show that in addition to the sign of the normal force slope $A$, its magnitude also appears to give further information on the stability of the prismatic body, although there are not quite sufficient data available at present to show this correlation clearly. This is one of the aspects that warrants further in-depth investigation. Finally, for all the shapes investigated in the present work, when the mean angle of attack increases, the transition in stability appears to follow the S→PU→U→S pattern.

## REFERENCES


1. G. V. Parkinson and N. P. H. Brooks 1961. *Journal of Applied Mechanics* **28**, 225. On the aeroelastic instability of bluff cylinders.
2. G. V. Parkinson and J. D. Smith 1964 *Quarterly Journal of Mechanics and Applied Mathematics* **17**, 225. The square prism as an aeroelastic non-linear oscillator.
3. P. W. Bearman and E. D. Obasaju 1982 *Journal of Fluid Mechanics* **119**, 297. An experimental study of pressure fluctuations on fixed and oscillating square section cylinders.
4. P. W. Bearman, I. S. Gartshore, D. J. Maull and G. V. Parkinson 1987 *Journal of Fluids and Structures* **1**, 19. Experiments on flow-induced vibration of a square-section cylinder.
5. P. W. Bearman and S. C. Luo 1988 *Journal of Fluids and Structures* **2**, 161. Investigation of the aerodynamic instability of a square-section cylinder by forced oscillation.
6. S. C. Luo, Md. G. Yazdani, Y. T. Chew and T. S. Lee 1994 *Journal of Wind Engineering and Industrial Aerodynamics* **53**, 375. Effects of incidence and afterbody shape on flow past bluff cylinders.
7. Md. G. Yazdani 1997 *Ph.D. Thesis*, *National University of Singapore*. Aerodynamic stability of prismatic bodies with various cross-sections.
8. H. P. A. H. Irwin, K. R. Cooper and R. Girrad 1979 *Journal of Wind Engineering and Industrial Aerodynamics* **5**, 93. Correction of distortion effects caused by tubing systems in measurements of fluctuating pressure.

9. S. C. Luo and T. L. Gan 1991 *Journal of The Institution of Engineers*, *Singapore* **31**, 33. Correction of distortion in fluctuating pressure signal caused by long pressure transmitting PVC tubing.

## APPENDIX: NOMENCLATURE

$A$ normal force slope $= \partial C_N/\partial\alpha$
$a$ amplitude of oscillation
$C_A$ axial force coefficient
$C_D$ drag force coefficient
$C_L$ lift force coefficient
$C_N$ normal force coefficient
$d$ cylinders' characteristic dimension
$f_N$ frequency of forced oscillation
$Re$ Reynolds number
$U$ free stream velocity
$U_r$ reduced velocity
$\alpha$ angle of incidence
$\mu$ dynamic viscosity of fluid
$\rho$ density of fluid